PNAS RESEARCH ARTICLE | ENVIRONMENTAL SCIENCES

Black carbon aerosols over Indian Ocean have unique source fingerprint and optical characteristics during monsoon season

Krishnakant Budhavant[a,b], August Andersson[c], H. Holmstrand[c], S. K. Satheesh[b], and Örjan Gustafsson[c,1]

Edited by Tami C. Bond, Colorado State University, Fort Collins, CO; received June 14, 2022; accepted January 7, 2023 by Editorial Board Member Akkihebbal R. Ravishankara

Effects of aerosols such as black carbon (BC) on climate and buildup of the monsoon over the Indian Ocean are insufficiently quantified. Uncertain contributions from various natural and anthropogenic sources impede our understanding. Here, we use observations over 5 y of BC and its isotopes at a remote island observatory in northern Indian Ocean to constrain loadings and sources during little-studied monsoon season. Carbon-14 data show a highly variable yet largely fossil (65 ± 15%) source mixture. Combining carbon-14 with carbon-13 reveals the impact of African savanna burning, which occasionally approach 50% (48 ± 9%) of the total BC loadings. The BC mass-absorption cross-section for this regime is 7.6 ± 2.6 m^2/g, with higher values during savanna fire input. Taken together, the combustion sources, longevity, and optical properties of BC aerosols over summertime Indian Ocean are different than the more-studied winter aerosol, with implications for chemical transport and climate model simulations of the Indian monsoon.

air pollution | black carbon | long-range transport | Asian aerosol

Aerosols remain one of the largest uncertainties in our current understanding of Earth's climate system (1). Within the chemically complex aerosol mixture, black carbon (BC) plays an important role as it is likely the most significant component that absorbs sunlight and thereby contributes to direct climate warming—in contrast to the overall cooling effect of aerosols. Furthermore, BC is also a cloud condensation nuclei (CCN), making BC–cloud interactions an additional modulator of climate impact, potentially countering the direct effects (2). The climate effects of BC remain highly uncertain, reflecting poorly constrained emission sources, optical properties, atmospheric transport, and aerosol–cloud interactions (2–4). Given its mean lifetime of around a week, the climate impact of BC is largely regional, and vast emissions from hotspot regions like South Asia and Africa may perturb both regional climate and the South Asian monsoon system over extensive scales of the northern Indian Ocean, with potentially devastating effects on the regions' agriculture and freshwater supply.

Despite its relatively short lifetime, BC is still ubiquitously observed far afield in the wider receptor regions of global emission hotspot regions such as those of South Asia, China, and Africa (Fig. 1). The vast expanse of the Indian Ocean makes the cumulative climate effects in this region comparably large. Meanwhile, the aged aerosol regime in this region may have different sources and aerosol properties compared with more well-studied anthropogenic emission hotspot regions. A major uncertainty in the climate effect of BC is related to the poorly constrained emission sources, with uncertainties typically exceeding a factor of two (5). These effects propagate when modeling climate effects in more remote areas since geographical emission footprint can be very large, while more local sources may have unproportionally large effects (5, 6). Another major source of uncertainty for BC is the variability in its light-absorption properties, (often reported as the mass-absorption coefficient; MAC), especially after aging and coating, induced during long-range transport (3, 7). While there have been substantial efforts focused on constraining this parameter, including changes from fresh BC particles to mixed states, or potential source-related differences, there appear to be large and poorly understood differences between geographical domains and physicochemical states with insufficient observations in the large-scale receptor systems of the Indian Ocean especially during the summer monsoon season (2, 3, 8, 9).

Observation-based source apportionment of BC based on carbon isotope ($\Delta^{14}C$ and $\Delta^{13}C$) techniques have been particularly informative as they combine high analytical precision with high source specificity (6, 10–12). Other source apportionment techniques for BC, such as molecular, ionic, and optical, are hampered by the fact that these indirect tracers are not part of the intrinsic BC chemical domain, and are just inferred by correlation, and thus are not conservative source tracers. In contrast, isotope techniques

Significance

This study of the Indian Ocean summer period pins down an aerosol regime that is geographically and compositionally different than the more studied winter period. The Indian Ocean summer aerosol regime is of greater relevance for the regionally important monsoon system of South Asia. Combining chemical, isotope, and optical properties with air mass transport analysis, the study resolves compositional source regimes for this vast marine domain during 2013 to 2017 with implications for the monsoon buildup and also for ecosystems, agriculture, and global warming. The fraction fossil of BC is more variable yet significantly larger (~65%) compared to for BC in wintertime South Asian outflow. Combining carbon-14 with stable isotopes revealed that savanna-burning fires from Africa periodically account for half of BC loadings over the Indian Ocean.

Author contributions: K.B. and Ö.G. designed research; K.B. and Ö.G. performed research; K.B., A.A., H.H., S.K.S., and Ö.G. contributed new reagents/analytic tools; K.B., A.A., and Ö.G. analyzed data; and K.B., A.A., H.H., S.K.S., and Ö.G. wrote the paper.

The authors declare no competing interest.

This article is a PNAS Direct Submission. T.C.B. is a guest editor invited by the Editorial Board.

[1]To whom correspondence may be addressed. Email: orjan.gustafsson@aces.su.se.

This article contains supporting information online at https://www.pnas.org/lookup/suppl/doi:10.1073/pnas.2210005120/-/DCSupplemental.

Published February 13, 2023.

conducted on thermochemical isolates of the actual BC fraction have been found powerful in various regions such as South Asia (10, 12, 13), East Asia (14, 15), and the Arctic (16–18) but not yet in the monsoon-forming summer season of South Asia.

Here, we use the Maldives Climate Observatory at Hanimaadhoo (MCOH) as a boreal summer large-scale receptor site in the Indian Ocean. The same site has been used in several studies to investigate the South Asian outflow for the winter season (6, 10, 19). This study focus on the much less investigated summer period, to characterize a geographically and compositionally different aerosol regime that is likely of greater relevance for the regionally important monsoon system of South Asia. Combining aerosol chemistry (carbonaceous components and inorganic ions) with carbon isotope and optical properties with air mass transport analysis, facilitates to resolve compositional source regimes—with diverse implications (e.g., on the ecosystem, agriculture productivity, visibility, global warming)—for this vast marine domain during five full summer monsoon seasons.

Results and Discussion

Atmospheric Transport. During the boreal summer (austral winter) the air mass-flow patterns over the northern Indian Ocean is mainly governed by southerly winds (7, 20, 21) (Fig. 1). During this time, the intertropical convergence zone is at its northernmost location, bringing monsoon rains to the South Asian region. Back-trajectory (BT) analysis for MCOH for the five summers of the present campaign agrees well with this climatological large-scale circulation pattern (*SI Appendix*, Fig. S3). During this time, the air was transported primarily from the central Indian Ocean and the Arabian Sea to the sampling site, yet also with some limited contact with anthropogenic sources (e.g., coastal areas, ocean traffic) during the 15 d prior to arrival (*SI Appendix*, Fig. S1).

Monsoon Season (Boreal Summer) Aerosol Composition. Atmospheric aerosols interact with clouds and influence the hydrological cycle, e.g., by acting as CCN. The aerosol composition during the summer season (Indian monsoon) in the northern Indian Ocean was investigated using a combined analysis of BC, organic carbon (OC), inorganic ions, and meteorological wind patterns (Table 1). Throughout the sampling period, BC and OC concentrations in $PM_{2.5}$ were 0.02 to 0.92 μg m^{-3} (average: 0.15 ± 0.15 μg m^{-3}) and 0.04 to 1.25 μg m^{-3} (average: 0.29 ± 0.25 μg m^{-3}), respectively (Fig. 2). BC concentrations were three times higher in Arabian air masses (0.25 ± 0.19 μg m^{-3}) than air masses stemming for the preceding 15 d from over the Indian Ocean (0.10 ± 0.12 μg m^{-3}) (Fig. 2). Overall, the mass concentrations of the carbonaceous aerosols are here constrained to be four to five times lower in the summer period than during the winter when high-pollution air masses are consistently brought to the region with northern air masses from the Indo Gangetic Plain (7, 13).

Particulate matter is either directly emitted or formed in the atmosphere as secondary inorganic aerosols and secondary organic aerosols. We found SO_4^{2-} was the most abundant inorganic ion species, followed by Cl^-, Na^+, Ca^{2+}, NH_4^+, K^+, NO_3^-, and Mg^{2+}. Higher concentrations of nss-SO_4^{2-} and NH_4^+ were associated with air masses from India's western and southern parts compared with when air masses spend more time over the ocean.

The ratios and correlations of different aerosol species provide information on sources and their atmospheric process. A correlation was observed between BC and OC (*SI Appendix*, Table S4: $R^2 = 0.6$, $P < 0.01$), which is lower than what is typically observed at MCOH during the dry winter period South Asian outflow regime. This likely reflects a more mixed source regime over the summertime Indian Ocean. The OC to BC ratios varied greatly from 0.6 to 9.7 (average: 3.4 ± 1.9) at MCOH (Fig. 2), likely affected by variability in both emission sources and in the processing during long-range transport (7, 19, 22). The nss-K^+ / BC is particularly high when the air masses stem from Australia and Africa (Fig. 3 and *SI Appendix*, Fig. S2), where biomass burning is common during the summer monsoon (11, 23). The mass ratios of NO_3^-/nss-SO_4^{2-} were 0.1 + 0.2, indicating a more significant contribution of nss-SO_4^{2-}. A good correlation of nss-SO_4^{2-} with NO_3^- indicates that maritime transportation (sea traffic) may be another source of SO_4^{2-}. This indicates that biomass burning emissions and maritime transportation may both affect the aerosol composition over the northern Indian Ocean.

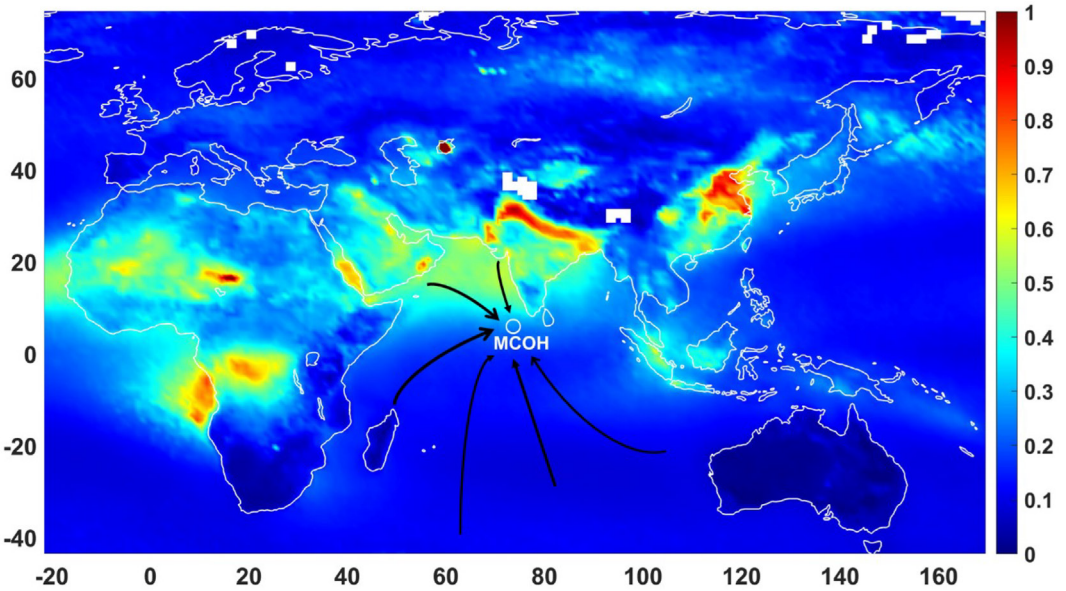

Fig. 1. Map depicting average AOD (AOD_{550}) from May to October (2013 to 2017). Black arrows indicate constrained air mass transport pathways to the MCOH in the northern Indian Ocean.

Table 1. Summary of aerosol parameters for the total summer period and for different airmass origins during the present Indian Ocean monsoon season campaigns. Mass absorption cross-section (MAC) of BC, the concentration of BC and OC, and various ionic concentrations in $PM_{2.5}$ were measured at the MCOH for two different 15-d air mass source sectors during the boreal summer (May to October 2013 to 2017)

	BC ($\mu g\ m^{-3}$)	BC-MAC$_{678}$ ($m^2\ g^{-1}$)	OC ($\mu g\ m^{-3}$)	nss-SO_4^{2-} ($\mu g\ m^{-3}$)	NO_3^- ($\mu g\ m^{-3}$)	nss-K^+ ($\mu g\ m^{-3}$)	NH_4^+ ($\mu g\ m^{-3}$)
Summer	0.2 ± 0.2	7.6 ± 2.5	0.3 ± 0.3	1.1 ± 1.0	0.1 ± 0.1	0.1 ± 0.2	0.2 ± 0.2
Arabian Sea	0.3 ± 0.2	6.2 ± 1.2	0.4 ± 0.3	1.4 ± 1.1	0.1 ± 0.2	0.2 ± 0.3	0.3 ± 0.3
Indian Ocean	0.1 ± 0.1	8.3 ± 2.6	0.2 ± 0.3	0.8 ± 0.6	0.1 ± 0.1	0.2 ± 0.1	0.1 ± 0.2

Dual Carbon-Isotope-Based Source Apportionment of BC in Monsoon-Season. The carbon-14 signature of BC can be used with high specificity and precision to constrain the fraction of BC stemming from biomass burning versus from fossil fuel combustion, Eq. 1. The isotope fingerprints for the five summers of the present study (Fig. 3) establishes a contribution from biomass burning of 35 ± 15%, with values ranging between 10% and 67% (*SI Appendix*, Table S1). This BC source apportionment for the summer monsoon season are both much more variable and more fossil than what is observed at the MCOH receptor region during the dry winter periods when the air masses predominantly represent the outflow from the Indian subcontinent (55 ± 5%) (6, 10, 12, 19). This demonstrates that the summertime Indian Ocean represents a quite different, and more fossil, BC source regime. The fossil contribution to BC likely comes from a mixture of ultimately land-based sources in South India, Arabia, and from at-sea traffic (e.g., shipping) on the Indian Ocean.

By combining these carbon-14 signatures with stable carbon ($\delta^{13}C$) isotope signatures, we can further refine the source contributions, by differentiating the biomass component into the fractions from C_3 and C_4 plants, Eq. 2. The C_3 are found in most biomes, while C_4 mainly grows in semidry, warm regions like savannas, and is also in certain agricultural crops (e.g., maize and sugarcane). Throughout the period, C_3 and fossil emissions dominate the sources of BC over the region (94 ± 2%). However, during three events both the $\Delta^{14}C$ and $\delta^{13}C$ signatures are simultaneously enriched in heavy isotopes, signaling an increase in relative contribution from incomplete combustion of C_4 plants/residues. Markov chain Monte Carlo (MCMC) simulations shows that during these events the C_4 source fraction is contributing 22 to 29% of the BC loading (Fig. 4).

A geographically resolved source apportionment of the different BC emissions is achieved by combining the source apportionment results with 15-d air mass transport back trajectory analysis. First excluding the three unusual and specific savanna-burning events with elevated C_4 contributions, we investigate if there are significant differences in the isotopic signatures of the two main air mass clusters: the Indian Ocean

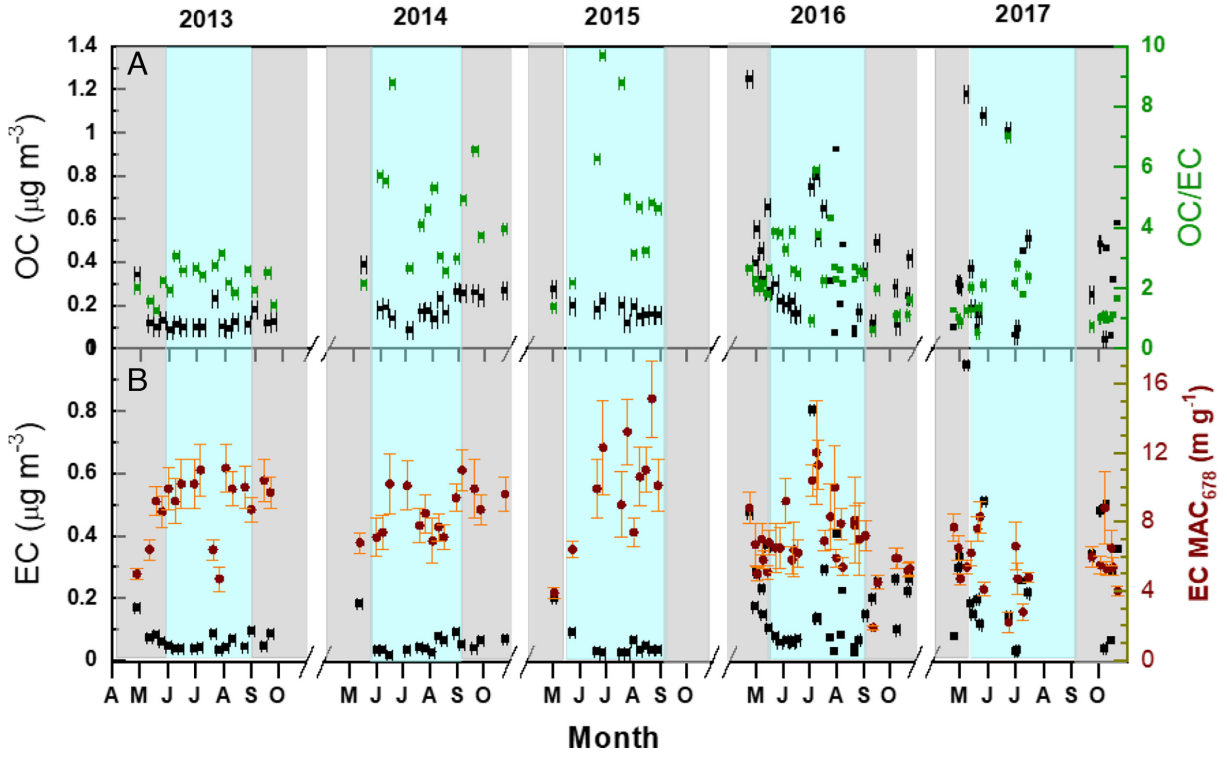

Fig. 2. Temporal patterns in $PM_{2.5}$ carbonaceous aerosol concentrations, elemental ratios, and optical properties during the summer/monsoon seasons of 2013 to 2017 for airmasses intercepted at MCOH. Panel *A* shows OC and OC/BC ratio while Panel *B* shows BC and BC-MAC at 678 nm. Horizontal and vertical line bars indicate one-SD. Vertical color-shaded fields indicate roughly the two key geographical source regions based on cluster back trajectory analysis: gray (Arabian Sea), and blue (Indian Ocean).

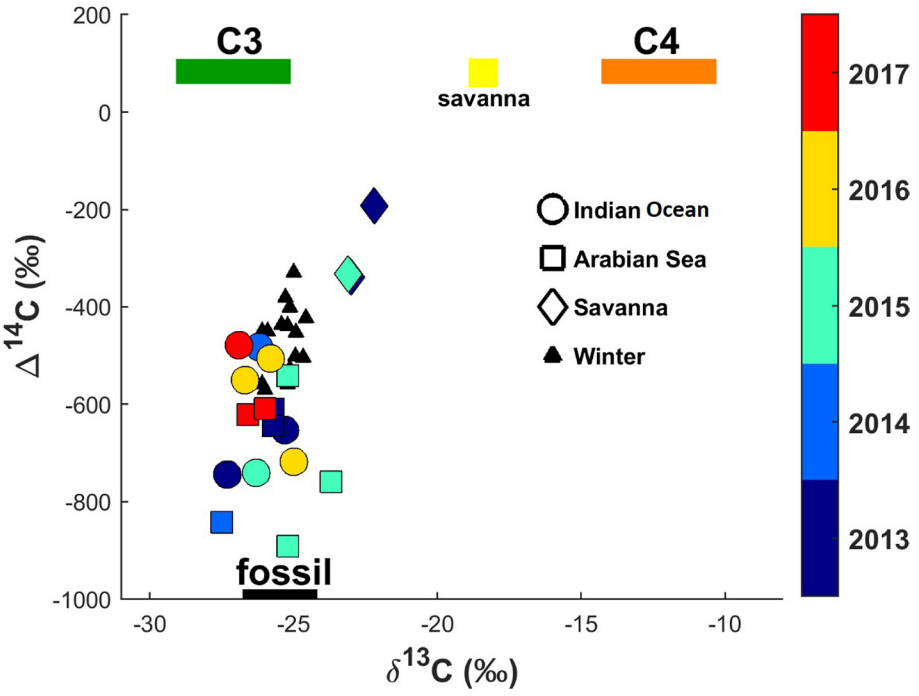

Fig. 3. Two-dimensional carbon isotope plot for BC intercepted at MCOH during summer/monsoon season. The colored symbols—circles, squares, and diamonds—represent summer samples for source clusters Indian Ocean; the Arabian Sea, and African savanna, respectively. The colors of these symbols represent the different years, according to the color bar. The black triangles represent, for comparison, winter-period data from 2012 and 2016 (6, 12). The colored boxes show the endmember (source-specific isotope values): fossil; C_3 plants and C_4 plants (size of box represents mean ± SD). The yellow "savanna" box represents an observation-based estimate of the isotopic values for savanna vegetations (27).

($\Delta^{14}C = -588 \pm 121‰$; $\delta^{13}C = -26.2 \pm 0.8‰$) and the Arabian Sea ($\Delta^{14}C = -689 \pm 126‰$; $\delta^{13}C = -25.7 \pm 1.1‰$). A *t* test analysis (two-tailed, heteroscedastic) suggests there are no significant differences for either isotope signature. Thus, the incoming air from the Indian Ocean and the Arabian Sea may be considered to be highly variable, but have similar emission source profiles.

Moving on to the three events with elevated contributions from incomplete combustion of C_4 plants, there may be two overall source types in this region causing enrichment in ^{13}C: SB emissions and anthropogenic emissions from C_4 agricultural crops. In wintertime MCOH, contributions from the burning of sugarcane (a C_4 plant) in southern India have been shown to be a small, but significant contributor to BC received over MCOH and thus the

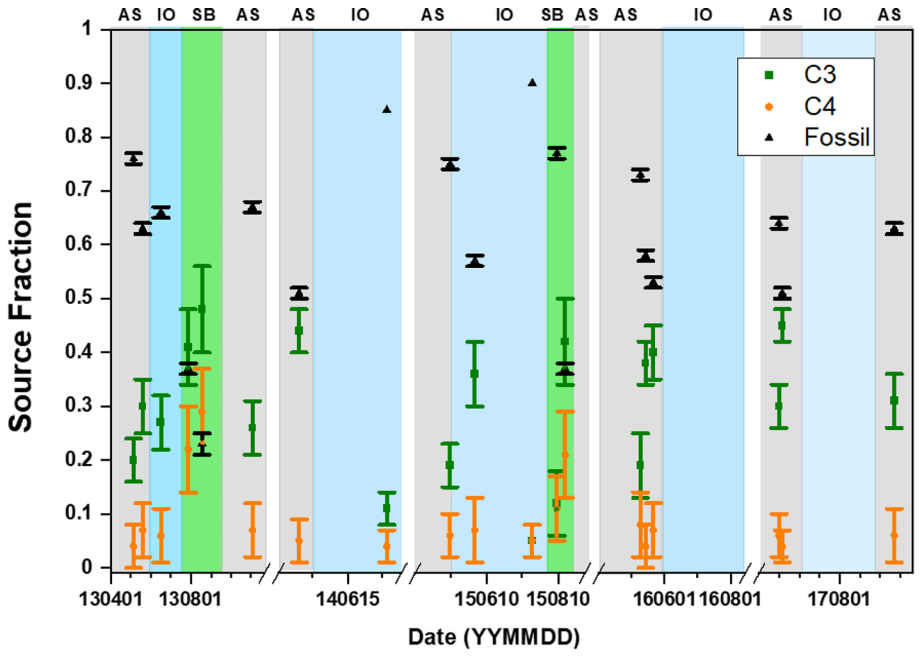

Fig. 4. Fractional source contributions to summer/monsoon BC from C_3 plants (green), C_4 plants (orange), and fossil sources (black). The error bars (one SD) were calculated using MCMC simulations. Vertical color-shaded fields indicate roughly three 15-d back trajectory source sectors: gray (Arabian Sea, AS), blue (Indian Ocean, IO), and green (influence by savanna burning, SB).

northern Indian Ocean (6). A common feature for the three specific summer-period events discussed here, however, is that for none of the BTs computed during the aerosol collection times (every 3 h, for filter collections of 1 to 2 wk) had the air mass passed over India, or belong to the Arabian Sea cluster. It is therefore unlikely that the BC in these summer-period samples are affected by anthropogenic activities in South Asia.

Savanna fires are therefore a more likely source of the C4-influenced BC for these three events. Surrounding the Indian Ocean are two regions with reoccurring savanna fires: Australia and sub-Saharan Africa. Analysis of overall aerosol optical depth (AOD) (Fig. 1) and sample-specific fire spot detections (FIRMS) suggests that during the boreal summer of the present study period, there are virtually no savanna fires (using AOD as a proxy) in Australia (which are more common in austral spring), while there are large-scale fires in southern Africa. Plumes from such have been reported to disperse eastbound over the southern Indian Ocean ("rivers of smoke") (23). A clear seasonal pattern (July to November) of pollution originating from biomass-burning plumes located in Africa and Madagascar has been established by both remote and in-situ observations of trace gases such as by measurements at the Reunion Island, southwest Indian Ocean (24, 25, 26). During the boreal summer when the intertropical convergence zone is at its northernmost point, it is conceivable that this pollution is intercepted and recorded by the measurements achieved at MCOH. It is therefore plausible that the events with elevated $\Delta^{14}C$ and $\delta^{13}C$ signatures reflect emissions from savanna fires in sub-Saharan Africa. This is also supported by analysis of satellite-based fire spot detection (FIRMS), which during specific sampling periods of the three elevated samples show clear fire signals in Africa, but not in Australia (*SI Appendix*, Fig. S6).

The relative contributions of C_4 plants to the total vegetation mass in savannas may be highly variable. However, as a guiding estimate, a value of 50% has been suggested for eastern Africa (27). Using this value, we can obtain a rough estimate of the fraction of BC from savanna fires by dividing the fraction C_4 with this number. During the three events with elevated carbon isotope signatures, the fraction from savanna fires was thus substantial and ranged from 42 to 58%. This conclusion is also supported by an increasing C_3 contribution during these events. This shows what a strong perturbation the emissions of BC from savanna fires in southern Africa may be—intercepted roughly 2,000 km away in the northern Indian Ocean—and that this earth system process has at times a large influence on the aerosols during the summer monsoon season.

An additional implication of the current study is that a substantial fraction of BC aerosols over the Indian Ocean has residence times exceeding 2 wk. The dual-isotope source apportionment yield that about one-third of the BC aerosols stems from biomass combustion, yet the extended back trajectory analyses suggest that the receiving air masses have resided over the ocean for the 15 d prior to arrival to the MCOH receptor location. Since biomass combustion must have occurred over land, this substantial biomass combustion fraction of the BC must have residence times exceeding 2 wk. This finding has implications for how BC aerosol residence time may be described in atmospheric chemistry and climate models, at least for the South Asian – Indian Ocean region.

The Mass Absorption Coefficient (MAC) of BC over Monsoon-Season Indian Ocean. The mass-absorption cross-section (MAC) is a key parameter in Mie calculations (proportional to the imaginary refractive index) and thereby for estimating the direct climate forcing of BC. The optical properties of BC in the ambient atmosphere is difficult to constrain using remote sensing, with large geographical and atmospheric processing variability (3, 4). Here, we find that during the whole five-summer observation-based study period, the measured BC MAC_{678} was 7.6 ± 2.6 m^2 g^{-1} (mean ± SD), with a range from 4.0 to 10.6 m^2 g^{-1} for the Indian monsoon season (*SI Appendix*, Fig. S5). The MAC may vary depending on sources but is also likely affected strongly by the internal mixing or coating state of the BC particles (9, 28), such that the MAC is enhanced (increases) with different types of coatings (3). Here, we do not find any clear relations between the MAC and loadings of inorganic ions or OC (*SI Appendix*, Fig. S8), suggesting an unresolved influence on the MAC. However, we do find a tendency that the MAC increase with the fraction C_4 (*SI Appendix*, Fig. S3). This suggests that the BC from savanna fire emissions may be more strongly absorbing than from other sources of aerosols to the Indian Ocean during the monsoon buildup phase, and therefore should be treated carefully when parameterizing large-scale atmospheric and climate models.

Taken together, this observation-based study, covering five full summer seasons at a remote Indian Ocean island observatory, demonstrates that the BC aerosol over the Indian Ocean has a different source fingerprint and different optical properties than earlier studied aerosol regimes from the wintertime continental outflow. The differences in chemical and light absorption properties of BC in summertime versus in winter may have repercussion both on the accuracy of current estimates of both aerosol radiative forcing and the effect of the aerosols in affecting the buildup of the Indian monsoon over the northern Indian Ocean during the summertime, with cascading effect on multiple environmental system operations in South Asia, such as rainfall.

Methods

Aerosol Sample Collection. The observatory campaign presented here were performed at MCOH (Lat 6.78°N long 73.18°E) during five summer monsoon seasons (May-October, 2012 to 2017) (Fig. 1). MCOH has been used for a diverse set of aerosol and radiation studies over its continual operation since 2004, yet very few studies focused on the summer period (7, 10, 20, 29, 30). Aerosol filter samples ($PM_{2.5}$: Particulate Matter < 2.5 μm aerodynamic diameter) were collected at the top of the observatory tower (15 m height). For this study, a total of 178 aerosol samples were collected on precombusted (450 °C) 150-mm diameter quartz filters (Millipore) using a high-volume sampler (DIGITEL Elektronik AG, Model DH77 at 500 L/min). Blank filters were shipped, stored, and processed identically as samples.

Measurement of Aerosol Carbon Speciation and Concentrations. The mass concentration of elemental carbon (EC, here referred to as BC), OC, and total carbon (TC = EC + OC) were measured with a thermal-optical transmission analyzer (Sunset Laboratory), using the National Institute for Occupational Safety and Health (NIOSH-5040) method (31, 32). After sample collection, filters were used for the chemical analysis using standard protocols and appropriate techniques (6, 12, 33). No detectable signal was observed for the BC in field blanks (n = 20). The OC concentration values were blank corrected by subtracting an average field black (5% of sample signals).

CO_2 isolation of BC Fraction and Subsequent $\Delta^{14}C$ and $\delta^{13}C$ Analysis. The BC was isolated from the filter sample via thermal-optical analysis and evolved CO_2 for the BC fraction was purified online and collected using a cryotrap as detailed elsewhere (34, 35). Analysis of the dual-carbon signature of $\delta^{13}C$ and $\Delta^{14}C$ provides direct insight into major BC emission source categories. Twenty aerosol samples were chosen to determine BC isotopic composition from receptor filters representing air masses arriving from constrained geographic regions around the Indian Ocean based on 15 d of air mass back trajectories (*SI Appendix*, Table S1). The CO_2 evolved from the BC combustion in the aerosol filter was diverted and purified online through magnesium perchlorate and silver wool traps to remove water and halogen-containing gases, respectively. Subsequently, it was

cryotrapped in liquid nitrogen followed by flame sealing in precombusted glass tubes. The CO_2 in the glass ampoules was converted to graphite and analyzed for radiocarbon and stable carbon isotopic composition at the Ångström Laboratory, Department of Nuclear Physics, Uppsala University, Sweden. The relative contribution to BC from biomass burning and fossil fuel combustion sources was calculated with an isotopic mass-balance equation

$$\Delta^{14}C = \Delta^{14}C_{biomass} \times f_{bio}\Delta^{14}C + \Delta^{14}C_{fossil} \times (1 - f_{bio}). \quad [1]$$

Here, $\Delta^{14}C_{obs}$ represents the radiocarbon signature in ambient samples. $\Delta^{14}C_{fossil}$ is −1,000‰, as it is completely depleted in ^{14}C. The $\Delta^{14}C$ of annual plants represented the signature of CO_2 for the collection year. In addition to $\Delta^{14}C$, the BC fingerprint was further distinguished by including the $\delta^{13}C$ signature in the analysis using the following isotopic mass balance relation (6, 11):

$$\begin{pmatrix} \Delta^{14}C_{obs} \\ \delta^{13}C_{obs} \\ 1 \end{pmatrix} = \begin{pmatrix} \Delta^{14}C_{C3} & \Delta^{14}C_{C4} & \Delta^{14}C_{fossl} \\ \delta^{13}C_{C3} & \delta^{13}C_{C4} & \delta^{13}C_{fossil} \\ 1 & 1 & 1 \end{pmatrix} \begin{pmatrix} f_{C3} \\ f_{C4} \\ f_{fossil} \end{pmatrix}, \quad [2]$$

where, the $\delta^{13}C$ signature allows us to differentiate the fraction biomass into C_3 plants (most terrestrial plants, e.g., trees and rice and wheat) and C_4 plants (e.g., sugarcane and many savanna grasses), such that $f_{bio} = f_{C3} + f_{C4}$. The fossil source may also be divided into different components, with different $\delta^{13}C$ signatures (e.g., liquid fossil; coal combustion or gas flaring; refs. 6, 12 and 22). However, a recent detailed analysis suggests that the main source at the current observation sites, the isotopic mixture, is dominated by the mixture of C_3 plants, C_4 plants, and liquid fossil (including at-sea shipping) (6). The stable carbon isotopic signatures for these sources (endmembers) were set to be: $\delta^{13}C_{fossil} = -25.5 \pm 1.3$‰, $\delta^{13}C_{C3} = -27.1 \pm 2$‰, $\delta^{13}C_{C4} = -13.1 \pm 1.2$‰. A Bayesian approach was used to account for the variability in the end members, and the results were calculated through MCMC simulations (*SI Appendix*, Table S2 and S3), using MATLAB version R2019b.

Absorption Measurements. The link between atmospheric concentration and direct radiative forcing by BC is its mass absorption cross-section (MAC). The laser beam (678 nm) of the Sunset Laboratory aerosol carbon analyzer was used to measure the light-attenuation [ATN = $-\ln(I/I_0)$] of the aerosols on the filter (36). The MAC_{BC} of BC is calculated as (37):

$$MAC_{BC} = \frac{ATN}{BC_{loading} \cdot MS \cdot R(ATN)}, \quad [3]$$

where R is the correction for nonlinearity emerging when measuring light absorption through a filter:

$$R = \left(\frac{1}{1.114} - 1\right)\left(\frac{\ln(ATN) - \ln(0.1)}{\ln(0.5) - \ln(0.1)}\right) + 1. \quad [4]$$

Here MS is an empirical multiple scattering correction factor implemented in most filter loading correction schemes. Here, a factor of 4.5 was chosen to estimate the multiple scattering effects. We used a screening protocol for our calculated MAC values: data points where the BC loadings were less than three times the estimated loading uncertainties (as the signal-to-noise was too low), while data points where *ATN* > 1 were also removed (to ensure the validity of the *ATN* correction term Eq. 4). All-in-all 33% of the data points were screened using this approach. The MACs for the screened data typically generated unrealistically high (>20 m^2/g) or low (<2 m^2/g) values. Uncertainties of the calculated MACs were generated through Monte Carlo-based error propagation, assuming the BC loading uncertainties are normal distributed.

Water-Soluble Ion Analysis. A portion of each aerosol filter was extracted with Milli-Q to analyze water-soluble inorganic ions (Na^+, K^+, Ca^{2+}, Mg^{2+}, NH_4^+, Cl^-, SO_4^{2-}, NO_3^-) using Ion Chromatograph (IC, Dionex Aquion). The system contains a guard column and an anion–cation separator column with a primary exchange resign and suppressor column (AERS500/CERS 500). The cation eluent consisted of methane sulfonic acid solution (20 mM), and the anion eluent consisted of sodium carbonate (Na_2CO_3) and sodium bicarbonate ($NaHCO_3$) solutions (1 M) prepared in distilled water. Quality assurance was performed based on field blanks, laboratory-produced test samples, and certified reference standards (Merck, ~1,000 ppm). Random error calculated from the analysis of synthetic samples in a batch and given as one-SD was 8% for cations and 5% for anions. All filter-based collected samples contained a certain amount of sea salt.

Air Mass Back-Trajectories and Remote Sensing. Various air mass source regions affected the sampling during BS, allowing a broad air mass classification (6,171 trajectories). The sampling site (MCOH) encountered air masses from multiple geographical areas during the BS (*SI Appendix*, Figs. S1 and S2). Fifteen-day air mass trajectories were generated from MCOH at an arrival height of 50 m, computed every 3 h, using the National Oceanic and Atmospheric Administration (NOAA) Hybrid Single-Particle Lagrangian Trajectory model (version 4). These individual trajectories were clustered into six geographical regions. Overall, we use these cluster analysis results to discuss BC's relative contribution over MCOH from various geographical domains. The MODIS (Moderate Resolution Imaging Spectroradiometer) satellite-derived FIRMS (Fire Information for Resource Management System)-based fire-count data were combined with cluster analysis to understand the impact of biomass burning emissions from potential source regions during the sampling period (*SI Appendix*, Fig. S2). The meteorological parameters were obtained from the Hanimaadhoo meteorological station (*SI Appendix*, Fig. S4), fulfilling the World Meteorological Organization standards (38).

Data, Materials, and Software Availability. The data on isotopic signatures of ambient BC, MAC, and source fraction of BC using MCMC simulations are provided in the *SI Appendix*. All other data are included in the article and/or *SI Appendix*.

ACKNOWLEDGMENTS. Elena Kirillova (Stockholm University) is acknowledged for her support during laboratory analysis. We thank the Maldives Meteorological Services of the Maldives government for supporting the operation of MCOH, especially Mr. Sharafulla Thoha, Miss. Mariyam, and Mr. Faruhaadh Moosa for collecting samples. K.B. give thanks for the additional support from the Asian Institute of Technology, Thailand. This work was supported by research grants from the Swedish Research Council for Sustainable Development (FORMAS Contract Nos. 942-2015-1061 and 2020-01917) and the Swedish Research Council (VR Contract Nos. 2015-03279; 2017-01601, and 2020-05384).

Author affiliations: [a]Maldives Climate Observatory at Hanimaadhoo, Maldives Meteorological Services, H. Dh. Hanimaadhoo 02020, Republic of Maldives; [b]Divecha Centre for Climate Change, Indian Institute of Science, Bangalore 560012, India; and [c]Department of Environmental Science, Bolin Centre for Climate Research, Stockholm University, Stockholm 10691, Sweden

1. IPCC, 2021: Climate Change 2021: The Physical Science basis. Contribution of working group I to the sixth assessment report of the Intergovernmental Panel on Climate Change, V. Masson, P. Zhai, A. Pirani, S.L. Connors, C. Pean *et al.*, Eds. (Cambridge University Press, 2021).
2. T. C. Bond *et al.*, Bounding the role of black carbon in the climate system: A scientific assessment. *J. Geophys. Res. Atmos.* **118**, 5380–5552 (2013).
3. Ö. Gustafsson, V. Ramanathan, Convergence on climate warming by black carbon aerosols. *Proc. Natl. Acad. Sci. U.S.A.* **113**, 4243–4245 (2016).
4. O. Boucher *et al.*, Jury is still out on the radiative forcing by black carbon. *Proc. Natl Acad. Sci. U.S.A.* **113**, 5092–5093 (2016).
5. P. Winiger *et al.*, Siberian Arctic black carbon sources constrained by model and observations. *Proc. Natl. Acad. Sci. U.S.A.* **114**, E1054–E1061 (2017).
6. S. Dasari *et al.*, Source quantification of South Asian black carbon aerosols with isotopes and modelling. *Environ. Sci. Technol.* **54**, 11771–11779 (2020).
7. K. Budhavant *et al.*, Enhanced light-absorption of black carbon in rainwater compared with aerosols over the northern Indian ocean. *J. Geophys. Res. Atmos.* **125**, e2019JD031246 (2020).

8. T. C. Bond, R. W. Bergstrom, Light absorption by carbonaceous particles: An investigative review. *Aerosol Sci. Technol.* **40**, 27–67 (2006).
9. M. Z. Jacobson, Strong radiative heating due to the mixing state of black carbon in atmospheric aerosols. *Nature* **409**, 695–697 (2001).
10. Ö. Gustafsson *et al.*, Brown clouds over South Asia: Biomass or Fossil fuel combustion? *Science* **323**, 495 (2009).
11. A. Andersson *et al.*, Seasonal source variability of carbonaceous aerosols at Rwanda Climate Observatory. *Atmos. Chem. Phys.* **20**, 4561–4573 (2020).
12. C. Bosch *et al.*, Source-diagnostic dual-isotope composition and optical properties of water-soluble organic carbon and elemental carbon in the South Asian outflow intercepted over the Indian Ocean. *J. Geophys. Res. Atmos.* **119**, 11743–11759 (2014).
13. K. Budhavant *et al.*, Radiocarbon-based source apportionment of elemental carbon aerosols at two South Asian receptor observatories over a full annual cycle. *Environ. Res. Lett.* **10**, 064004 (2015).
14. H. Ni *et al.*, Source apportionment of carbonaceous aerosols in Xi'an, China: Insights from a full year of measurements of radiocarbon and stable isotopes 13C. *Atmos. Chem. Phys.* **18**, 16363–16383 (2018).
15. M. Li, Source apportionment of carbonaceous aerosols in the diverse atmospheric environment of China by dual-carbon isotope method. *Sci. Total Environ.* **806**, 150654 (2022).
16. P. Winiger *et al.*, Source apportionment of Circum-Arctic atmospheric black carbon from isotopes and modeling. *Sci. Adv.* **5**, eaau8052 (2019).
17. P. Winiger *et al.*, Isotope-based source apportionment of EC aerosol particles during winter high-pollution events at the Zeppelin Observatory, Svalbard. *Environ. Sci. Technol.* **49**, 11959–11966 (2015).
18. T. E. Barrett *et al.*, Source contributions to wintertime elemental and organic carbon in the Western Arctic based on radiocarbon and tracer apportionment. *Environ. Sci. Technol.* **49**, 11631–11639 (2015).
19. S. Dasari *et al.*, Photochemical degradation affects the light absorption of water-soluble brown carbon in the south Asian outflow. *Sci. Adv.* **5**, eaau8066 (2019).
20. J. Kesti *et al.*, Changes in aerosol size distributions over the Indian ocean during different meteorological conditions. *Tellus B* **72**, 1–14 (2020).
21. M. G. Lawrence, J. Lelieveld, Atmospheric pollutants outflow from southern Aisa: A review. *Atmos. Chem. Phys.* **10**, 11017–11096 (2010).
22. E. N. Kirillova *et al.*, 13C- and 14C-based study of sources and atmospheric processing of water-soluble organic carbon (WSOC) in south Asian aerosols. *J. Geophys. Res. Atmos.* **118**, 614–626 (2013).
23. R. J. Swap *et al.*, Africa burning: A thematic analysis of the southern African regional science initiative (SAFARI 2000). *J Geophys. Res.* **108**, 8465 (2003).
24. L. Kirago *et al.*, Atmospheric black carbon loadings and sources over Eastern Sub-Saharan Africa are governed by the regional savanna fires. *Environ. Sci. Technol.* **56**, 15460–15469 (2022), 10.1021/acs.est.2c05837.
25. V. Duflot *et al.*, Analysis of the origin of the distribution of CO in the subtropical southern Indian Ocean in 2007. *J. Geophys. Res.-Atmos.* **115**, D22106 (2010).
26. M. Zhou *et al.*, Atmospheric CO and CH4 time series and seasonal variations on Reunion Island from ground-based in situ and FTIR (NDACC and TCCON) measurements. *Atmos. Chem. Phys.* **18**, 13881–13901 (2018).
27. S. Callewaert *et al.*, Analysis of CO_2, CH_4, and CO surface and column concentrations observed at Réunion Island by assessing WRF-Chem simulations. *Atmos. Chem. Phys.* **22**, 7763–7792 (2022).
28. F. Liu *et al.*, Review of recent literature on the light absorption properties of black carbon: Refractive index, mass absorption cross-section, and absorption function. *Aerosol Sci. Technol.* **54**, 33–51 (2020).
29. C. E. Corrigan *et al.*, Impact of monsoon transition on the physical and optical properties of aerosols. *J. Geophys. Res.* **111**, D18208 (2006).
30. V. Ramanathan *et al.*, Atmospheric brown clouds: Hemispherical and regional variations in long-range transport, absorption, and radiative forcing. *J. Geophys. Res.* **112**, D22S21 (2007).
31. M. E. Birch, R. A. Cary, Elemental carbon-based method for monitoring occupational exposures to particulate diesel exhaust. *Aerosol Sci. Technol.* **25**, 221–241 (1996).
32. Z. Zencak *et al.*, Quantification and radiocarbon source apportionment of black carbon in atmospheric aerosols using the CTO-375 method. *Atmos. Environ.* **41**, 7895–7906 (2007).
33. E. N. Kirillova *et al.*, 13C- and 14C-based study of sources and atmospheric processing of water-soluble organic carbon (WSOC) in south Asian aerosols. *J. Geophys. Res. Atmos.* **118**, 614–626 (2013).
34. B. Chen *et al.*, Source forensics of black carbon aerosols from China. *Environ. Sci. Technol.* **47**, 9102–9108 (2013).
35. A. Andersson *et al.*, Regionally-varying combustion sources of the January 2013 severe haze events over easter china. *Environ. Sci. Technol.* **49**, 2038–2043 (2015).
36. K. Ram, M. M. Sarin, Absorption coefficient and site-specific mass absorption efficiency of elemental carbon in aerosols over Urban, Rural, and high-altitude sites in India. *Environ. Sci. Technol.* **43**, 8233–8239 (2009).
37. E. Weingartner *et al.*, Absorption of light by soot particles: Determination of the absorption coefficient using aethalometers. *J. Aerosol. Sci.* **34**, 1445–1463 (2003).
38. World Meteorological Organization, *International Meteorological Vocabulary* Geneva, WMO-No. 182, 1992).